

Cold interactions between an Yb^+ ion and a Li atom: Prospects for sympathetic cooling, radiative association, and Feshbach resonances

Michał Tomza,^{1,2} Christiane P. Koch,² and Robert Moszynski¹

¹*Faculty of Chemistry, University of Warsaw, Pasteura 1, 02-093 Warsaw, Poland*

²*Theoretische Physik, Universität Kassel, Heinrich-Plett-Str. 40, 34132 Kassel, Germany*

(Dated: December 7, 2024)

The electronic structure of the $(\text{LiYb})^+$ molecular ion is investigated with two variants of the coupled cluster method restricted to single, double, and noniterative or linear triple excitations. Potential energy curves for the ground and excited states, permanent and transition electric dipole movements, and long-range interaction coefficients C_4 and C_6 are reported. The data is subsequently employed in scattering calculations and photoassociation studies. Feshbach resonances are shown to be measurable despite the ion's micromotion in the Paul trap. Molecular ions can be formed in their singlet electronic ground state by one-photon photoassociation and in triplet states by two-photon photoassociation; and control of cold atom-ion chemistry based on Feshbach resonances should be feasible. Conditions for sympathetic cooling of an Yb^+ ion by an ultracold gas of Li atoms are found to be favorable in the temperature range of 10 mK to 10 nK; and further improvements using Feshbach resonances should be possible. Overall, these results suggest excellent prospects for building a quantum simulator with ultracold Yb^+ ions and Li atoms.

PACS numbers: 34.70.+e, 34.50.Cx, 33.80.-b, 34.20.-b

I. INTRODUCTION

Trapped ions are a highly controllable system with strong interactions and thus find many applications, for example in precision measurements, quantum computing or quantum sensing [1–3]. Currently, a growing number of experiments combines trapped ions with ultracold atoms [4–14], allowing to study the dynamics of a single ion immersed in an atomic Bose-Einstein condensate [4] or to control chemical reactions of a single ion and ultracold atoms [6]. Further prospects include the idea to build a quantum simulator with a hybrid system of ultracold ions and atoms to emulate solid-state physics [15, 16] or to form ultracold molecular ions [17].

Any experimental proposal based on a hybrid system of ultracold ions and atoms has to face two issues. The first one is the choice of trapping method for the ions; the second one potential losses due to chemical reactions between ions and atoms. Although optical traps for ions become available [18, 19], radio-frequency (rf) based Paul traps still constitute the most popular choice [20]. Unfortunately, the time-dependent rf potential induces micromotion of the ion that limits the minimum temperature that can be achieved [21–23].

The impact of the micromotion can be minimized by choosing a large ion to atom mass ratio [21]. An Yb^+ ion immersed in an ultracold gas of Li atoms is thus a perfect candidate to construct a hybrid ion-atom experiment. Besides the large ion to atom mass ratio to facilitate cooling, the relatively simple electronic structure of the $(\text{LiYb})^+$ molecular ion, with the entrance channel $\text{Yb}^+(^2S)+\text{Li}(^2S)$ well separated from other electronic states, reduces potential nonradiative losses. Nevertheless, to estimate the rates for radiative loss as well as the ratio of elastic to inelastic collision cross sections, reliable knowledge of the electronic structure is needed.

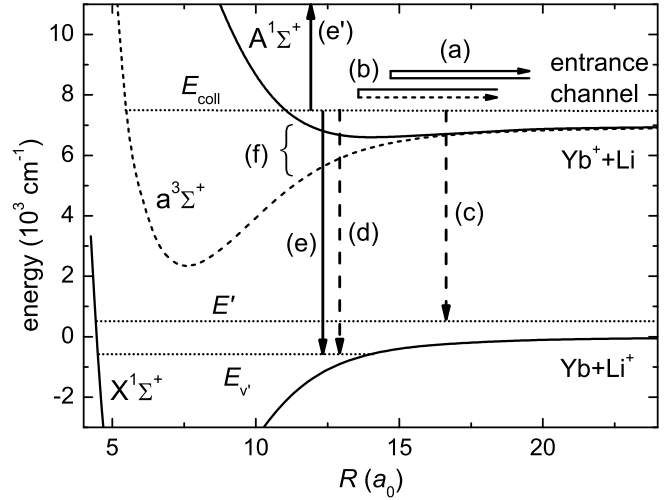


FIG. 1. Interaction between an Yb^+ ion and a Li atom. The collision can entail the following processes: elastic scattering (a), superelastic (spin-changing) scattering (b), radiative charge transfer (c), radiative association (d), photoassociation to ground (e) or excited (e') states, and Feshbach resonance based magnetoassociation (f).

This is essential both for realizing sympathetic cooling of the ion by the atoms [4, 5] and for coupling a crystal of trapped Yb^+ ions to a cloud of ultracold fermionic Li atoms, as proposed for building a quantum simulator to emulate solid-state physics [16]. All relevant processes are schematically summarized in Fig. 1.

To the best of our knowledge, the electronic structure and collisional properties of the Yb^+ ion interacting with the Li atom have not yet been investigated theoretically. Here we fill this gap and report an *ab initio* study of the

interactions of the Yb^+ ion with the Li atom, the system of interest in an ongoing experiment [24]. First, we investigate the electronic structure of the $(\text{LiYb})^+$ molecular ion by means of state-of-the-art *ab initio* techniques. Next, we employ the electronic structure data to investigate the prospects for sympathetic cooling, spontaneous radiative association, laser-induced association (photoassociation), and observation of Feshbach resonances. Special attention is paid to the formation of molecular ions by means of both spontaneous radiative association as well as stimulated photoassociation and to the control of chemical reactivity with both laser and magnetic fields.

The plan of our paper is as follows. Section II describes the theoretical methods used in the electronic structure and scattering calculations. Section III presents the results of the *ab initio* calculations in Sec. III A, followed by a discussion of elastic collisions, radiative charge transfer, radiative association, and Feshbach resonances in Secs. III B to III E. A critical assessment of our findings in view of their implication for experiment, in particular in terms of the prospects for sympathetic cooling and chemical reaction control, is provided in Sec. IV and Sec. V summarizes our paper.

II. COMPUTATIONAL DETAILS

A. Electronic structure calculations

We adopt the computational scheme successfully applied to the ground and excited states of the SrYb [25] and Sr_2 [26] molecules as well as the $(\text{BaRb})^+$ molecular ion [27]. The potential energy curve for the $X^1\Sigma^+$ ground electronic state is obtained with the coupled cluster method restricted to single, double, and noniterative triple excitations (CCSD(T)) method [28]. Potential energy curves for the first states in the $^3\Sigma$ and $^3\Pi$ symmetries are obtained with the spin-restricted open-shell coupled cluster method restricted to single, double, and noniterative triple excitations (RCCSD(T)) [29]. Cal-

culations of all other excited states employ the linear response theory (equation of motion) within the coupled cluster singles, doubles, and linear triples framework (LRCC3) [30, 31]. The basis set superposition error is eliminated by using the counterpoise correction of Boys and Bernardi [32]. The CCSD(T) and RCCSD(T) calculations were performed with the MOLPRO suite of codes [33], while LRCC3 calculations were carried out with the DALTON program [34].

The lithium atom is described by the augmented core-valence correlation consistent polarized valence quadrupole- ζ quality basis set, aug-cc-pCVQZ. For the ytterbium atom, the fully relativistic small-core energy consistent pseudopotential, ECP28MDF [35], and associated basis set, $(15s14p12d11f8g)/[8s8p7d7f5g]$, are employed. Due to the less efficient numerical code for the LRCC3 method it was computationally not feasible to carry out calculations for excited states correlating all electrons included in the model and using the large basis set. Therefore in these calculations, the core electrons are frozen and only the 12 outer-shells electrons are correlated.

The long-range asymptotics of the potentials is computed from Eqs. (4)–(8) of Ref. [27]. The dynamic polarizability at imaginary frequency of the Yb^+ ion and the Li atom are obtained by using the explicitly connected representation of the expectation value and polarization propagator within the coupled cluster method [36, 37] and the best approximation within the coupled cluster method XCCSD4 [38]. The dynamic polarizability at imaginary frequency of the Li atom is taken from Ref. [39] and the dynamic polarizability of the Yb^+ ion is obtained from the sum over state expression using the transition moments [40]. The static quadrupole polarizabilities of the Li and Yb atoms are taken from accurate atomic calculations reported in Refs. [41] and [42], respectively.

B. Scattering calculations

The Hamiltonian describing the nuclear motion in the $(\text{LiYb})^+$ system reads

$$\hat{H} = -\frac{\hbar^2}{2\mu} \frac{1}{R} \frac{d^2}{dR^2} R + \frac{\hat{l}^2}{2\mu R^2} + \sum_{S, M_S} V_S(R) |S, M_S\rangle \langle S, M_S| + V^{ss}(R) + V^{so}(R) + \hat{H}_{\text{Yb}^+} + \hat{H}_{\text{Li}}, \quad (1)$$

where R is the internuclear distance, \hat{l} the rotational angular momentum operator, μ the reduced mass, and $V_S(R)$ the potential energy curve for the state with total electronic spin S . The relativistic terms $V^{ss}(R)$ and $V^{so}(R)$ stand, respectively, for the spin-dipole-spin-dipole interaction responsible for the dipolar relaxation [43] and the second-order spin-orbit term [44]. The atomic Hamiltonian, \hat{H}_j ($j = \text{Yb}^+, \text{Li}$), including Zeeman

and hyperfine interactions is given by

$$\hat{H}_j = \zeta_j \hat{i}_j \cdot \hat{s}_j + \left(g_e \mu_B \hat{s}_{j,z} + g_j \mu_N \hat{i}_{j,z} \right) B \quad (2)$$

with \hat{s}_j and \hat{i}_j the electron and nuclear spin operators, ζ_j denoting the hyperfine coupling constant, $g_{e/j}$ the electron and nuclear g factors, and $\mu_{B/N}$ the Bohr and nuclear magnetons. For the fermionic Yb^+ ion, Eq. (2) re-

duces to the electronic Zeeman term. We neglect the unknown second-order spin-orbit coupling $V^{so}(R)$ but this does not affect the present analysis since the spin-spin coupling $V^{ss}(R)$ has a similar effect [43, 44].

The bound rovibrational levels are calculated by diagonalizing the nuclear Hamiltonian represented on a Fourier grid with adaptive step size [45–47]. The total scattering wave function is constructed in a fully uncoupled basis set,

$$|i_{Yb+}, m_{i,Yb+}\rangle |s_{Yb+}, m_{s,Yb+}\rangle |i_{Li}, m_{i,Li}\rangle |s_{Li}, m_{s,Li}\rangle |l, m_l\rangle,$$

with m_j the projection of angular momentum j on the space-fixed Z axis, assuming the projection of the total angular momentum $M_{tot} = m_{f,Yb+} + m_{f,Li} + m_l = m_{i,Yb+} + m_{s,Yb+} + m_{i,Li} + m_{s,Li} + m_l$, to be conserved. The coupled channels equations are solved using a renormalized Numerov propagator [48] with step-size doubling and about 100 step points per de Broglie wave length. The wave function ratio Ψ_{i+1}/Ψ_i at the i th grid step is propagated to large interatomic separations, transformed to the diagonal basis, and the K and S matrices are extracted by imposing long-range scattering boundary conditions in terms of Bessel functions.

The rate constant for elastic collisions in the i th channel is given by the diagonal elements of the S matrix summed over partial waves l ,

$$K_{el}^i(E) = \frac{\pi\hbar}{\mu k} \sum_{l=0}^{\infty} (2l+1) |1 - S_{ii}^l(E)|^2, \quad (3)$$

where $k = \sqrt{2\mu E/\hbar}$ with collision energy E . Similarly, the scattering length is obtained from the S matrix,

$$a = \frac{1}{ik} \frac{1 - S_{11}}{1 + S_{11}}. \quad (4)$$

Spontaneous radiative processes are governed by the Einstein coefficients. For the transitions between two bound rovibrational states vl and $v'l'$, scattering state of energy E and bound state $v'l'$, and two scattering states of energies E and E' , they are given by

$$A_{vl,v'l'} = \frac{4\alpha^3}{3e^4\hbar^2} H_l(E_{vl} - E_{v'l'})^3 \left| \langle \Psi_{vl} | d(R) | \Psi_{v'l'} \rangle \right|^2 \quad (5a)$$

$$A_{El,v'l'} = \frac{4\alpha^3}{3e^4\hbar^2} H_l(E - E_{v'l'})^3 \left| \langle \Psi_{El} | d(R) | \Psi_{v'l'} \rangle \right|^2 \quad (5b)$$

$$A_{El,E'l'} = \frac{4\alpha^3}{3e^4\hbar^2} H_l(E - E')^3 \left| \langle \Psi_{El} | d(R) | \Psi_{E'l'} \rangle \right|^2, \quad (5c)$$

respectively. In Eq. (5) the primed and unprimed quantities pertain to the ground and excited state potentials, respectively, $d(R)$ is the transition dipole moment from the ground to the excited electronic state, α the fine structure constant, and e the electron charge. The Hönl-London factor H_l is equal to $(l+1)/(2l+1)$ for the P branch ($l = l' - 1$), and to $l/(2l+1)$ for the R branch ($l = l' + 1$).

Radiative charge transfer can be described by the following Fermi golden rule type expression for the rate constant [49–51],

$$K_{CT}(E) = \frac{4\pi^2\hbar^2}{\mu k} \sum_{l=0}^{\infty} (2l+1) \sum_{l'=l\pm 1} \int_0^{\infty} A_{El,E'l'} d\varepsilon, \quad (6)$$

where $\varepsilon = E - E'$. Analogously, the rate constant for radiative association is given by

$$K_{RA}(E) = \frac{4\pi^2\hbar^2}{\mu k} \sum_{l=0}^{\infty} (2l+1) \sum_{l'=l\pm 1} \sum_{v'} A_{El,v'l'}. \quad (7)$$

The total rate constant for the radiative losses is the sum of Eqs. (6) and (7),

$$K_R(E) = K_{CR}(E) + K_{RA}(E). \quad (8)$$

Stimulated radiative association (photoassociation) becomes possible by applying a laser field. The rate constant for the photoassociation reads [52, 53]

$$K_{PA}(\omega, E) = \frac{\pi\hbar}{\mu k} \sum_l (2l+1) \sum_{v'l'} |S_{v'l'}(E, l, \omega)|^2, \quad (9)$$

with

$$|S_{v'l'}(E, l, \omega)|^2 = \frac{\gamma_{v'l'}^s(E, l) \gamma_{v'l'}^d}{(E - \Delta_{v'l'}(\omega))^2 + \frac{1}{4}[\gamma_{v'l'}^s(E, l) + \gamma_{v'l'}^d]^2}, \quad (10)$$

where $\gamma_{v'l'}^s(E, l)$ is the stimulated emission rate, and $\gamma_{v'l'}^d$ the rate for spontaneous decay, both in units of \hbar . $\Delta_{v'l'}(\omega)$ is the detuning relative to the position of the bound rovibrational level $v'l'$, i.e., $\Delta_{v'l'} = E_{v'l'} - \hbar\omega$ with $E_{v'l'}$ the binding energy of level $v'l'$. The spontaneous emission rates $\gamma_{v'l'}^d$ are obtained from the Einstein coefficients $A_{v'l',vl}$,

$$\gamma_{v'l'}^d = \sum_{vl} A_{v'l',vl} + \sum_l \int_0^{\infty} A_{v'l',El} d\varepsilon. \quad (11)$$

At low laser intensity I , the stimulated emission rate is given by the Fermi golden rule expression

$$\gamma_{v'l'}^s(E, l) = 4\pi^2 \frac{I}{c} (2l'+1) H_{l'} \left| \langle \Psi_{El} | d(R) | \Psi_{v'l'} \rangle \right|^2. \quad (12)$$

Equations (6), (7), and (9) give rate constants for a single scattering energy E . In practice, we have an ensemble of thermally populated states and the rate constants at a temperature T are obtained by performing a Boltzmann average,

$$K(T) = \frac{2}{\sqrt{\pi}(k_B T)^{3/2}} \int_0^{\infty} K(E) \sqrt{E} e^{-E/k_B T} dE. \quad (13)$$

III. NUMERICAL RESULTS AND DISCUSSION

A. Potential energy curves, permanent and transition electric dipole moments

Before presenting our potential energy curves, and permanent and transition dipole moments, we first compare the computed atomic results to the best available experimental data. Our predicted position of the nonrelativistic 2P state of the Li atom is 14910 cm^{-1} , to be compared with the experimental value of 14904 cm^{-1} [54]. For the 3P state of the Yb atom we obtain 17635 cm^{-1} , in a relatively good agreement with the experimental value of 18903 cm^{-1} [54]. The predicted ionization potentials (IP) are 43464 cm^{-1} for Li and 50267 cm^{-1} for Yb, in a good agreement with the experimental values of 43487 cm^{-1} and 50443 cm^{-1} [54], respectively. To further assess the quality of the methods, basis sets, and pseudopotential employed in the present work, we have computed the static polarizabilities of the ground state of the Li and Yb atoms and of the ground state of the Li^+ and Yb^+ ions. Our calculated polarizability of the Li atom ground state amounts 164.3 a.u. . The experimental value is $164.0 \pm 3.4\text{ a.u.}$ [55], while the best theoretical result is 164.0 a.u. [39]. Also the static polarizability of the Li^+ ion, 0.190 a.u. , is in a very good agreement with the experimental value of $0.188 \pm 0.002\text{ a.u.}$ [56]. Our static polarizabilities of the Yb atom and Yb^+ ion, 143.9 a.u. and 63.6 a.u. , also are in a very good agreement with the most sophisticated atomic calculations, giving $141 \pm 6\text{ a.u.}$ [57] and 62.04 a.u. [40], respectively.

The potential energy curves for the ground and excited states of the $(\text{LiYb})^+$ molecular ion are presented in Fig. 2, and the spectroscopic characteristics are reported in Table I. The transition and permanent electric dipole moments are plotted in Fig. 3 and Fig. 4, respectively. The leading long-range coefficients for the dispersion and induction interactions between the Li^+ ion and the Yb atom and between the Yb^+ ion and the Li atom, all in the ground electronic state, are reported in Table II.

The interaction of the ground-state Li^+ ion with the ground-state ytterbium atom results in single $X^1\Sigma^+$ electronic ground state of the $(\text{LiYb})^+$ molecular ion, cf. Fig. 2. The interaction between ion and atom is dominated by the induction contribution that results in the large binding energy of 9412 cm^{-1} , with the equilibrium distance equal to 6.2 bohr . The interaction of the ground-state Yb^+ ion with the ground-state Li atom, which both are open-shell, results in the two electronic states $a^3\Sigma^+$ and $A^1\Sigma^+$. The triplet state is strongly bound with binding energy equal to 4609 cm^{-1} , whereas the singlet potential is weakly bound by only 358 cm^{-1} . The large binding energy of the triplet a state as compared to that of the singlet A state can be rationalized in the molecular orbitals picture where the triplet state is stabilized by an admixture of the antibonding orbital correlated with the lowest asymptote.

Experimental proposals to immerse a ground state yt-

TABLE I. Spectroscopic characteristics of the $(\text{LiYb})^+$ molecular ion: equilibrium bond lengths R_e , well depths D_e , harmonic constants ω_0 , and rotational constants B_0 (for the isotope $^7\text{Li}^{172}\text{Yb}^+$).

State	R_e (bohr)	D_e (cm^{-1})	ω_0 (cm^{-1})	B_0 (cm^{-1})
$\text{Li}^+(^1S)+\text{Yb}(^1S)$:				
$X^1\Sigma^+$	6.20	9412	231	0.23
$\text{Li}(^1S)+\text{Yb}^+(^2S)$:				
$A^1\Sigma^+$	14.04	358	37.1	0.045
$a^3\Sigma^+$	7.59	4609	140	0.16
$\text{Li}^+(^1S)+\text{Yb}(^3P)$:				
$b^3\Pi$	5.83	8130	232	0.26
$c^3\Sigma^+$	12.46	3177	60.9	0.057
$\text{Li}(^2P)+\text{Yb}^+(^2S)$:				
$B^1\Sigma^+$	14.02	1332	50.1	0.045
$C^1\Pi$	6.71	1025	138	0.20
$e^3\Pi$	7.05	640	170	0.18
$d^3\Sigma^+$	7.56	426	218	0.16
$d^3\Sigma^+$	19.93	267	24.4	0.022

TABLE II. Induction and dispersion coefficients describing the long-range part of the interaction potential between the Li^+ ion and the Yb atom and between the Yb^+ ion and the Li atom, all in the ground electronic state.

System	C_4^{ind} (a.u.)	C_6^{ind} (a.u.)	C_6^{disp} (a.u.)
Li^++Yb	72.0	1280	6.4
Yb^++Li	82.1	711.7	711

terbium ion in a gas of ultracold ground state lithium atoms rely on negligible losses due to the atom-ion interaction. In this respect, our electronic structure results, Fig. 2, are promising since the corresponding electronic states, $a^3\Sigma^+$ and $A^1\Sigma^+$, are well separated from all other electronic states. This suggests that potential losses due to reactive collisions should be smaller than those predicted and observed in ultracold collisions of the Ba^+ ion with ultracold Rb atoms where the strong spin-relaxation was observed due to the spin-orbit coupling of both the incoming singlet $A^1\Sigma^+$ and triplet $a^3\Sigma^+$ states with the $b^3\Pi$ state at short internuclear separation [6, 7, 27].

The absolute value of the permanent electric dipole moments in Fig. 4 increases with internuclear distance. This is typical for heteronuclear molecular ions. It implies that, in contrast to neutral molecules, even very weakly bound molecular ions will have significant permanent electric dipole moment. The dotted lines in Fig. 4 represent the two limiting cases where the charge is completely localized on one of the atoms. The difference between the dotted lines and the calculated values can be understood as the interaction-induced variation of the permanent dipole moment [58] or the degree of charge delocalization. Asymptotically, the permanent dipole mo-

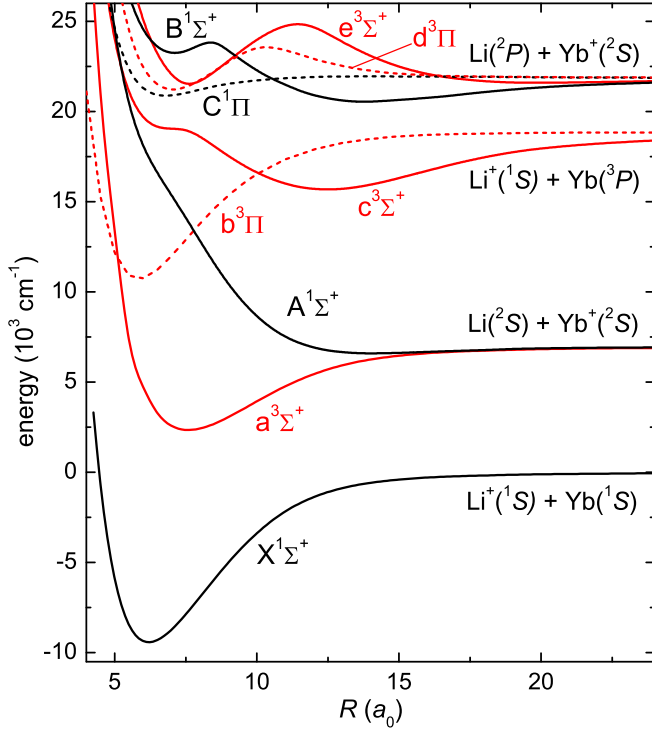


FIG. 2. (Color online) Non-relativistic potential energy curves of the $(\text{LiYb})^+$ molecular ion.

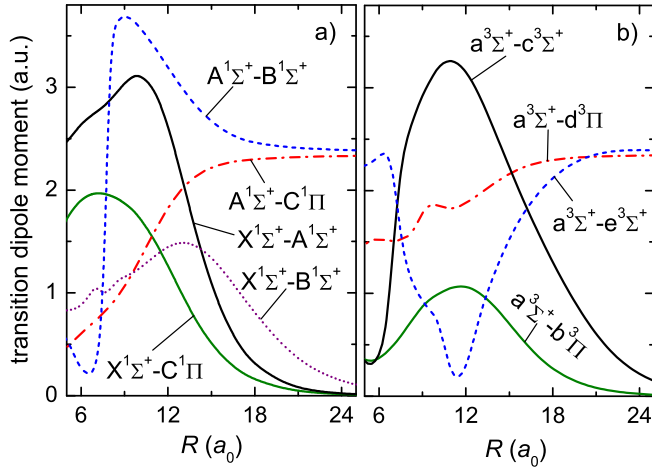


FIG. 3. (Color online) Transition electric dipole moments between singlet (a) and triplet (b) states of the $(\text{LiYb})^+$ molecular ion.

ments for all electronic states have to approach one of the two limiting cases.

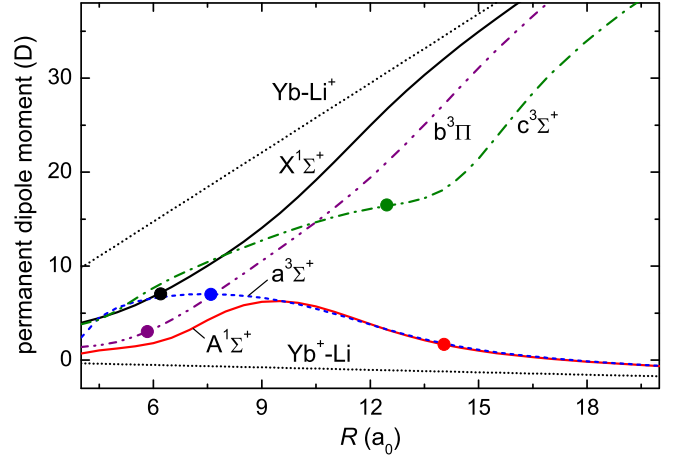


FIG. 4. (Color online) Permanent electric dipole moments of the most relevant singlet and triplet states of the $(\text{LiYb})^+$ molecular ion. The z -axis is oriented from Yb to Li and the origin is in the center of mass. The points indicate the values for the ground rovibrational level; and the dotted lines represent the permanent dipole moment that the molecular ion would have if the charge was completely localized on one of the atoms.

B. Elastic collisions

Ab initio electronic structure calculations do not provide sufficiently accurate interaction potentials to predict scattering lengths. We therefore calculate the scattering properties for a few isotopic mixtures with correspondingly different scattering lengths. For our *ab initio* data, the low energy s -wave scattering length in the $A^1\Sigma^+$ ($a^3\Sigma^+$) state amounts to $-385 a_0$ ($-695 a_0$) for $^{174}\text{Yb}^+ + ^6\text{Li}$ and to $2625 a_0$ ($982 a_0$) for $^{174}\text{Yb}^+ + ^7\text{Li}$. For $^{173}\text{Yb}^+ + ^6\text{Li}$ and $^{173}\text{Yb}^+ + ^7\text{Li}$ the low energy s -wave scattering length in the $A^1\Sigma^+$ ($a^3\Sigma^+$) state amounts to $-371 a_0$ ($-659 a_0$) and $2705 a_0$ ($1042 a_0$), respectively. These numbers have to be compared to the characteristic length scale of the atom-ion interaction which is given by $\sqrt{2\mu C_4/\hbar}$ and amounts to $1218 a_0$ for $(\text{LiYb})^+$. Therefore, the $^{174}\text{Yb}^+ + ^6\text{Li}$ isotope corresponds to small background scattering length and $^{174}\text{Yb}^+ + ^7\text{Li}$ to a large one.

Elastic collision rate constants are reported in Fig. 5. For collision energies larger than $10 \mu\text{K}$, when more partial waves contribute to the scattering process, the total rate of elastic collisions is similar for all isotopic mixtures, of the order of $10^{-8} \text{ cm}^3/\text{s}$, cf. Fig. 5. At lower energies, the elastic collision rates are decreased by two to three orders of magnitude, depending on scattering length and spin symmetry. Sympathetic cooling will be possible if the ratio of the rates for elastic to all inelastic or reactive collisions is larger than roughly a factor of 100. The rates for all inelastic processes are reported in the following sections.

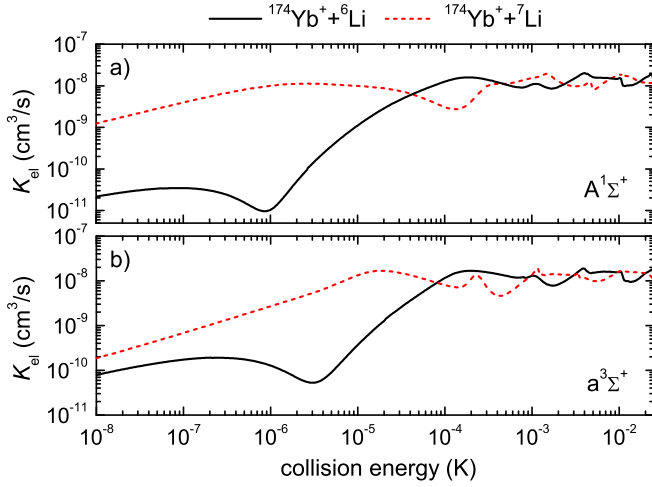
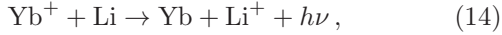


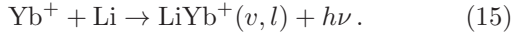
FIG. 5. Elastic scattering rates for collisions in the $A^1\Sigma^+$ (a) and $a^3\Sigma^+$ (b) electronic states. The $^{174}\text{Yb}^+ + ^6\text{Li}$ isotope (black solid lines) corresponds to small background scattering length, the $^{174}\text{Yb}^+ + ^7\text{Li}$ isotope (red dashed lines) to a large one.

C. Radiative charge transfer and radiative association

The $A^1\Sigma^+$ electronic state is directly coupled to the ground $X^1\Sigma^+$ electronic state by the electric transition dipole moment. This coupling is responsible for potential inelastic losses due to spontaneous radiative charge transfer (CT),



or radiative association (RA),



It can also be used for laser-induced molecule formation, i.e., photoassociation (PA),



to the singlet state. The $a^3\Sigma^+$ state is coupled by the electric transition dipole moment with the excited $b^3\Pi$ and $c^3\Sigma^+$ states. These couplings can be used for photoassociation to the triplet states.

Figure 6 presents the rate constants for radiative losses in collisions of the $^{174}\text{Yb}^+$ ion with ^6Li and ^7Li atoms in the $A^1\Sigma^+$ electronic state. The rates depend on the presence of resonances in the entrance channel. With rate constants two orders of magnitude larger than for radiative charge transfer, radiative association represents the main source of radiative loss. At the same time, the rates for radiative loss are comparatively small, 10^3 to 10^5 times smaller than the rates for the elastic scattering for temperatures below 10 mK, cf. Fig. 5. Radiative losses can further be reduced by several orders of magnitude

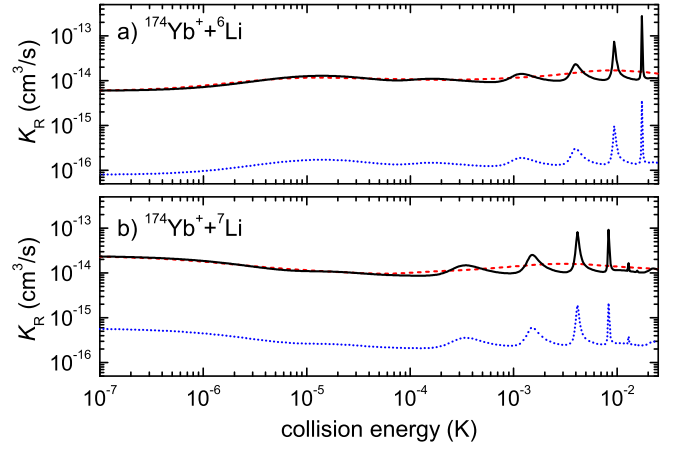


FIG. 6. (Color online) Rates for radiative association (black solid lines) and radiative charge transfer (blue dotted lines) for collisions of an $^{174}\text{Yb}^+$ ion with ^6Li and ^7Li atoms. The red dashed envelopes are the thermally averaged rates.

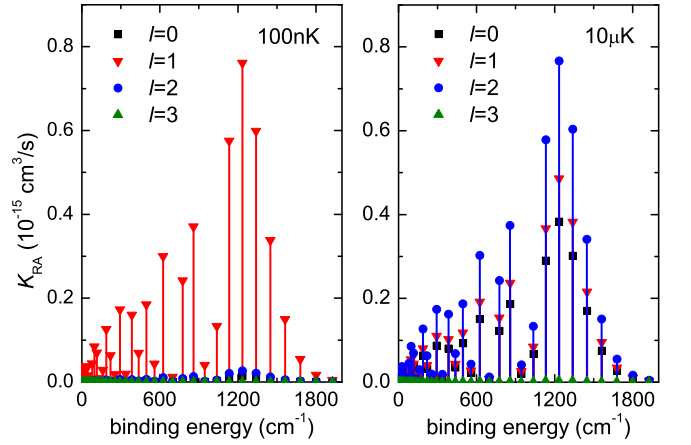


FIG. 7. (Color online) Radiative association rate vs binding energy of the final vibrational level in the $X^1\Sigma^+$ ground electronic state for an $^{174}\text{Yb}^+$ ion colliding with a ^6Li atom in the $A^1\Sigma^+$ state plotted at a temperature corresponding to 100 nK (left panel) and to $10 \mu\text{K}$ (right panel).

by applying an external magnetic field which restricts the collisional dynamics of the Yb^+ ion and the Li atom to the high-spin $a^3\Sigma^+$ state. Since there is no radiative loss channel for the triplet state, the only radiative losses for collisions in magnetic field will originate from an admixture of the $A^1\Sigma^+$ state. For an electronic state with a high-spin reference function, the admixture of a singlet state is given by the long-range dipolar spin-spin interaction and the spin-orbit coupling with higher excited states. Both appear in second order of perturbation theory, so they are very small. For these reasons, radiative losses should not pose a problem for sympathetic cooling of Yb^+ ions by a gas of ultracold Li atoms, especially if an external magnetic field is applied.

Radiative association is further analyzed in Fig. 7 which shows the RA rates to different rovibrational levels of the $(^6\text{Li}^{174}\text{Yb})^+$ molecular ion at temperatures of $T = 100$ nK and 10 μK . As expected, at low temperatures the radiative association is dominated by the contribution of s -wave collisions only, whereas at higher temperatures more partial waves come into play. The RA spectra for other isotopes have very similar shapes as those shown in Fig. 7 but the amplitudes of the rates vary due to the presence of resonances in the entrance channel. Interestingly, the largest partial rates are found for relatively strongly bound vibrational levels with binding energies of about 1200 cm^{-1} . Spontaneous radiative association can thus be used to produce the $(\text{LiYb})^+$ molecular ions. In next sections we will show that the molecule formation rates can be controlled by means of a laser field in photoassociation or by a magnetic field modifying Feshbach resonances. The latter is similar to Feshbach-optimized photoassociation of neutral molecules [59].

D. Photoassociation

In a controlled way, the $(\text{LiYb})^+$ molecular ions can be produced by applying a laser field to drive the association process. If the colliding Yb^+ ion and Li atom interact via the $A^1\Sigma^+$ electronic state, photoassociation to the $X^1\Sigma^+$ state is possible with a laser wavelength between 611 nm and 1438 nm. If the atom and ion are in the $a^3\Sigma^+$ state, photoassociation into the manifold of the $b^3\Pi$ and $c^3\Sigma^+$ states can be induced with laser wavelengths between 834 nm and 1140 nm. Since the triplet molecules are formed in an electronically excited state, they are subject to comparatively fast spontaneous decay, whereas the singlet molecules in the electronic ground state are more stable.

Photoassociation spectra for a $^6\text{Li}^{174}\text{Yb}^+$ are presented in Fig. 8(a) and Fig. 8(b) for the singlet and triplet spin symmetries, respectively. In both cases, and similarly to the radiative association discussed above, relatively strongly bound rovibrational levels can be populated, with binding energies of about 1200 cm^{-1} and about 1500 cm^{-1} for the singlet and triplet symmetries, respectively. It is not feasible to produce singlet state $(\text{LiYb})^+$ molecular ions with larger binding energy by using a one-photon transition since the $A^1\Sigma^+$ electronic state is repulsive at the equilibrium distance of the $X^1\Sigma^+$ ground electronic state. The largest photoassociation rates for the triplet state $(\text{LiYb})^+$ molecular ion are found for ions with a dominant $c^3\Sigma^+$ state component close to the equilibrium internuclear distance. The formation of the triplet state $(\text{LiYb})^+$ molecular ions dominated by the $b^3\Pi$ state component close to the equilibrium internuclear distance with a binding energy of about 7000 cm^{-1} is possible, but the rates for these transitions are three orders of magnitude smaller than the rates for transitions to the levels dominated by the $c^3\Sigma^+$ state component. It is worth noting that the characteristics of the photoasso-

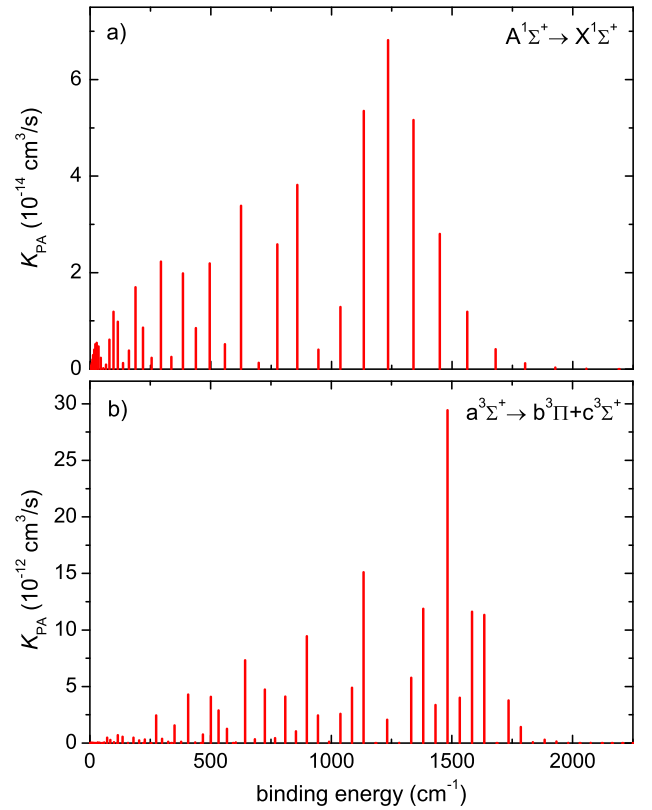


FIG. 8. (Color online) Photoassociation rates for rovibrational levels in the $X^1\Sigma^+$ ground electronic state and $A^1\Sigma^+$ state collisions of $^{174}\text{Yb}^+$ ions with ^6Li atoms (upper panel) and for rovibrational levels in the $c^1\Sigma^+$ and $b^3\Pi$ states and $a^3\Sigma^+$ state collisions (lower panel) for a laser intensity of $I = 100$ W/cm^2 and a temperature of 10 μK .

ciation spectra for $(\text{LiYb})^+$ presented in Fig. 8 are common for all ion-atom systems when both atom and ion are in the 2S electronic state.

The controlled formation of molecular ions is feasible only if the rates for the photoassociation (Fig. 8) are larger than those for radiative losses (Fig. 7). For the investigated system of Yb^+ ion and Li atom, this condition is met. Additionally, the photoassociation rate can be enhanced by controlling the magnetic Feshbach resonances [59] which are investigated in the next section.

E. Feshbach resonances

Two types of magnetically tunable Feshbach resonances between the Yb^+ ion and the Li atom exist, depending on the structure of the Yb^+ ion: (i) Bosonic Yb^+ ions ($^{171}\text{Yb}^+$ and $^{173}\text{Yb}^+$) have a non-zero nuclear spin. As a consequence, they possess a hyperfine manifold, such that Feshbach resonances between bosonic Yb^+ ions and Li atoms are of the same nature as those between two alkali metal atoms [60]. (ii) Fermionic Yb^+ ions do

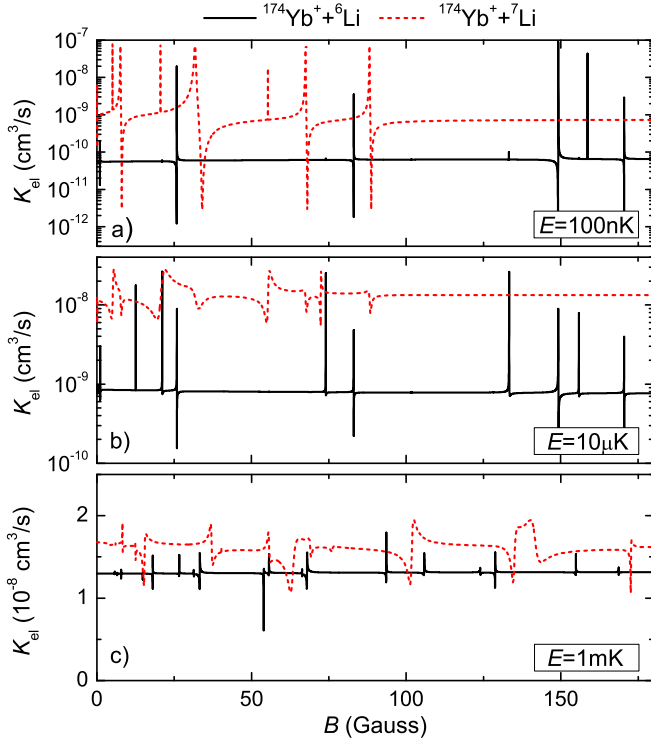


FIG. 9. (Color online) Elastic scattering rate constant vs magnetic field for collisions of fermionic $^{174}\text{Yb}^+$ ($\frac{1}{2}, -\frac{1}{2}$) ions with ^6Li ($\frac{1}{2}, \frac{1}{2}$) atoms and ^7Li ($1, 1$) atoms for collision energies corresponding to 100 nK, 10 μK , and 1 mK. Note the different y -axis scales.

not have nuclear spin and therefore they do not possess any hyperfine structure. Feshbach resonances between the fermionic Yb^+ ions and Li atoms result from the interaction of the hyperfine structure of the Li atom with the electronic spin of the Yb^+ ion [61]. The density of the Feshbach resonances at small magnetic fields in the latter case is larger as compared to the former case, cf. Fig. 9 and Fig. 10.

Figure 9 shows the rates for the elastic scattering of the fermionic $^{174}\text{Yb}^+$ ion in the $(f, m_f) = (\frac{1}{2}, -\frac{1}{2})$ state with fermionic ^6Li ($\frac{1}{2}, \frac{1}{2}$) and bosonic ^7Li ($1, 1$) atoms for collision energies corresponding to 100 nK, 10 μK , and 1 mK as a function of the external magnetic field. Contributions from the lowest three, seven, and fifteen partial waves are included, respectively, at these three energies. The density of Feshbach resonances for the fermionic ^6Li atom is larger as compared to bosonic ^7Li because the fermionic atom has a smaller hyperfine splitting than the bosonic one, 228.2 MHz versus 803.5 MHz. The scattering at a temperature of 100 nK and below is dominated by the s -wave collisions. The large Feshbach resonances visible in Fig. 9(a) are almost pure s -wave resonances, whereas the very narrow resonances are of p -wave character. At the temperature of 10 μK , s -wave and p -wave collisions contribute equally, cf. Fig. 9(b), and at tem-

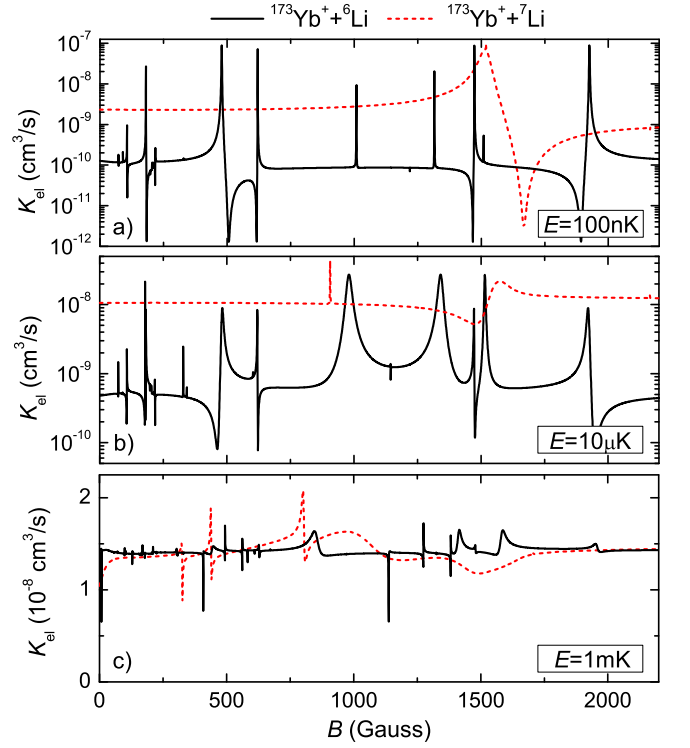


FIG. 10. (Color online) Elastic scattering rate vs magnetic field for collisions of bosonic $^{173}\text{Yb}^+$ ($3, -3$) ions with ^6Li ($\frac{1}{2}, \frac{1}{2}$) atoms and ^7Li ($1, -1$) atoms for collision energies corresponding to 100 nK, 10 μK , and 1 mK.

peratures above 100 μK , more partial waves start to contribute to the elastic scattering. At a temperature of 1 mK, as presented in Fig. 9(c), the elastic scattering is dominated by higher partial waves ($l = 3$ and $l = 4$) which wash out the resonance structure of the lower partial waves. Thus the Feshbach resonances visible in Fig. 9(c) are narrower and have much smaller amplitude as compared to those at lower temperatures.

Elastic scattering rates for bosonic $^{173}\text{Yb}^+$ ($3, -3$) ions and fermionic ^6Li ($\frac{1}{2}, \frac{1}{2}$) atoms, respectively, bosonic ^7Li ($1, -1$) atoms as a function of the external magnetic field are shown in Fig. 10 for collision energies of 100 nK, 10 μK , and 1 mK. Similarly to the case of the fermionic $^{174}\text{Yb}^+$ ion, cf. Fig. 9, scattering at a temperature of 100 nK is dominated by s -wave collisions with a few narrow p -wave resonances visible. At 10 μK , s -wave and p -wave collisions contribute equally and at temperatures above 1 mK many partial waves contribute to the rate of the elastic scattering. The structure and strength of the Feshbach resonances at temperatures above 1 mK is washed out by dominant contributions of higher partial waves to the total elastic scattering rate.

Finally, Figs. 11 and 12 present the rates for radiative losses, that is, radiative association and radiative charge transfer, as a function of magnetic field for collisions of the same species at the same temperatures as in

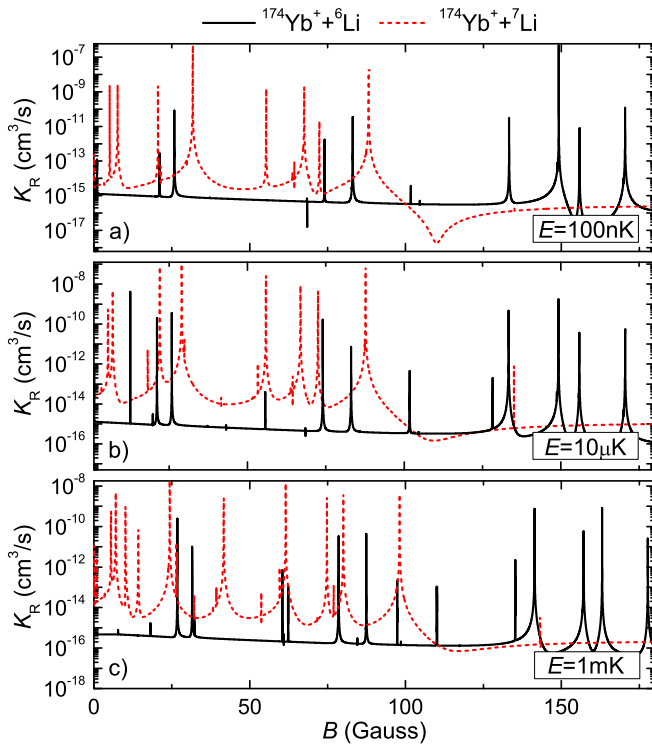


FIG. 11. (Color online) Radiative loss rate vs magnetic field for collisions between $^{174}\text{Yb}^+$ ($\frac{1}{2}, -\frac{1}{2}$) ions and ^6Li ($\frac{1}{2}, \frac{1}{2}$), respectively, ^7Li ($1, 1$) atoms for collision energies corresponding to 100 nK, 10 μK , and 1 mK.

Figs. 9 and 10. In contrast to the elastic scattering rates, Feshbach and shape resonances are clearly visible for all investigated temperatures. For all conditions the typical rates for elastic scattering are at least three orders of magnitude larger than the rates for radiative losses.

Comparing Figs. 9 and 10 to Figs. 11 and 12, a different temperature dependence of the rates for elastic scattering and radiative losses is observed. This can be understood by analyzing the mechanisms of the two processes: The elastic rates are dominated by the reflection from the long range potential. For higher partial waves with a large centrifugal barrier which dominates at high collision energies, the appearance of Feshbach resonances is strongly suppressed. By contrast, radiative losses occur at short internuclear distance only. For high partial waves, this requires tunneling through the centrifugal barrier. The probability of tunneling decays exponentially with the height of the centrifugal barrier. Therefore, at higher temperatures, higher partial waves contribute less to the radiative losses than to elastic scattering.

For other isotopes, both fermionic and bosonic ones, the characteristics of Feshbach resonances are similar to those discussed above. In particular, they depend on the choice of the entrance channel characterized by the hyperfine states of atom and ion. Different isotopes of Yb can be used to control the structure of Feshbach reso-

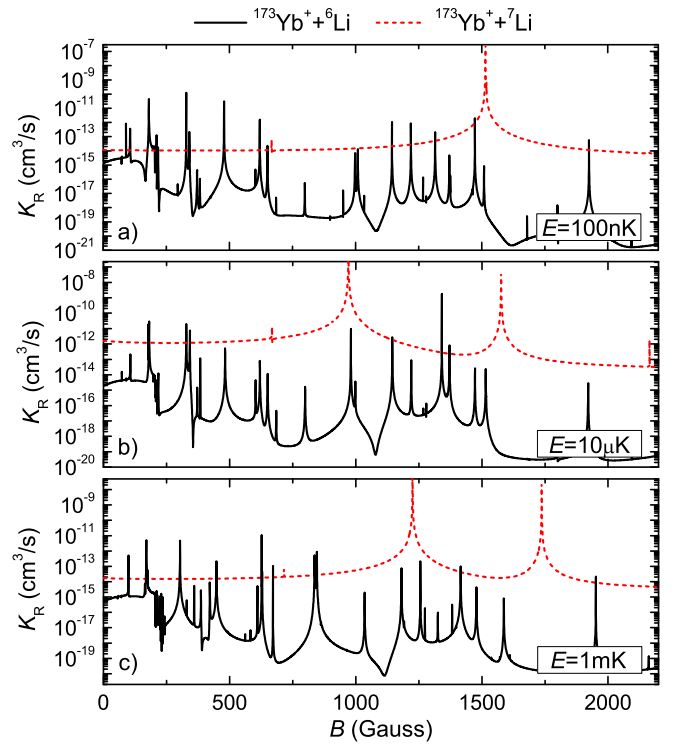


FIG. 12. (Color online) Radiative loss rate vs magnetic field for collisions between $^{173}\text{Yb}^+$ ($3, -3$) ions and ^6Li ($\frac{1}{2}, \frac{1}{2}$), respectively, ^7Li ($1, -1$) atoms for collision energies corresponding to 100 nK, 10 μK , and 1 mK.

nances due to the different masses.

IV. DISCUSSION

Since even the best state of the art *ab initio* methods cannot provide a reliable estimate of the *s*-wave scattering length, and since for $(\text{LiYb})^+$ it has not yet been measured, it is important to assess the dependency of our results on this quantity. Most severely, a different value of the scattering length than that obtained with our data might compromise our conclusions for sympathetic cooling. Comparison of Figs. 5 and 6 suggests sympathetic cooling to be feasible since the elastic cross section is three to five orders larger than the cross section for all inelastic processes in the relevant temperature range. If the true background scattering length is very small, smaller than that for $^{174}\text{Yb}+^6\text{Li}$ (red dashed lines in Fig. 5 and upper panel in Fig. 6), the elastic rate constant will be smaller, at the same time the inelastic losses will also be smaller, due to the decreasing amplitude of the scattering wave function in the entrance channel. This can be estimated, for example, using Eq. (25) of Ref. [27]. As a result, even for scattering lengths smaller than that of $^{174}\text{Yb}+^6\text{Li}$ in our calculations, the ratio of elastic to inelastic rate constants should still be of the

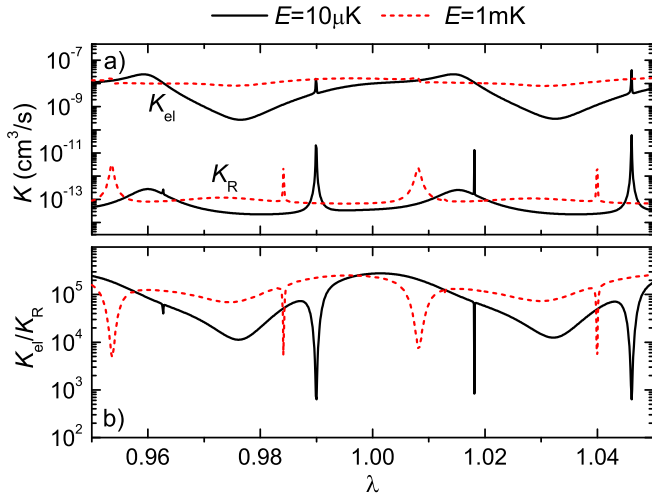


FIG. 13. (Color online) Sensitivity of the rate constants for elastic scattering K_{el} and radiative association and charge transfer K_R (a) and of the ratio of elastic to inelastic rate constants (b) at collision energies of $10\ \mu\text{K}$ (black solid lines) and 1 mK (red dashed lines) to a scaling factor λ applied to the interaction potential, $V(R) \rightarrow \lambda \cdot V(R)$.

order of at least 100 for temperatures between 10 nK and 10 mK . However, for higher temperatures, when many partial waves contribute, the overall rate constants do not strongly depend on the s -wave scattering length unless a strong shape resonance appears. It is well known that the position and especially the width of a resonance depend very sensitively on the fine details of the interaction potential, even if the bound rovibrational states are correctly located by *ab initio* calculations [62]. To assess the sensitivity of the scattering results on the uncertainty of the interaction potential, we follow the approach employed, among others, in Ref. [63, 64]. Specifically, we have carried out calculations with the interaction potential scaled by a constant factor λ in the range 0.95 to 1.05 . This scaling factor roughly corresponds to the estimated error bounds in the calculated potential energy curves. The results are shown in Fig. 13 for the collision energies of $10\ \mu\text{K}$ and 1 mK . An inspection of this figure shows that the weak dependence of the cross sections on the potential scaling λ is only disturbed by the presence of sharp resonances that occur when bound states of $(\text{LiYb})^+$ cross the incoming threshold as a function of λ . Fig. 13 shows that the resonances occur in narrow ranges of λ , so that there is a low probability that the true potential will be such that the ratio of elastic to inelastic cross sections is seriously affected by resonances for collision energies below 1 mK . Last but not least, the ratio of the elastic to the inelastic cross section is always much larger than 100, showing that within the grid of λ employed in the present calculations there is a strong evidence that the sympathetic cooling the Yb^+ ion by the laser-cooled Li atoms is possible. It is worth noting

that the effect of resonances on the rate constants will be additionally washed out by the Boltzmann averaging [65].

This statement can be made even stronger by exploiting the magnetic field dependence of the scattering length. Figures 11 and 12 show minima in the radiative loss constants, for example close to 160 G in Fig. 11 (top and middle panel). Tuning the magnetic field to such a value will enhance the ratio of elastic to inelastic rate constants by a factor of 1000 and should yield very efficient sympathetic cooling. Another option consists in tuning the magnetic field close to one of the broader Feshbach resonances, observed in Figs. 9 and 10, to increase the elastic rate constant while keeping inelastic losses at bay. The exact positions of Feshbach resonances will depend on the true scattering lengths but the characteristics of presented results is general and depends mainly on the actual hyperfine structure and nature of colliding ion and atom.

The magnetic field dependence can also be employed to enhance the inelastic rate constants, in case one is interested in the observation of cold chemical reactions. If the field-free scattering length is essentially zero, this will also decrease the inelastic rate constants, as explained above. The remedy then is to tune the magnetic field to a value where a maximum in K_R is observed, cf. Figs. 11 and 12. Alternatively, one could also make use of minima in the elastic rate constants, cf. Fig. 9, which will decrease the ratio of the rate constants by up to a factor of 1000. The latter is not applicable at higher temperatures ($> 10\ \mu\text{K}$) where the Feshbach resonances are less pronounced in the elastic rate constant.

V. SUMMARY AND CONCLUSIONS

We have carried out state of the art *ab initio* calculations to determine the electronic structure of the $(\text{LiYb})^+$ molecular ion. Potential energy curves, transition and permanent electric dipole moments, and long range coefficients were calculated. Good agreement between our computed atomic results and the available experimental data was obtained.

The entrance channels for collisions between the $\text{Yb}^+(^2S)$ ion and the $\text{Li}(^2S)$ atom are found to be well separated from all other electronic states, suggesting comparatively small losses due to reactive collisions. Significant permanent electric dipole moments are obtained, even for very weakly bound states of the molecular ion. This opens the way for various control schemes. For example, a non-resonant laser field will lead to a strong Stark effect that can be used to control energy level shifts state-selectively. This should enable state-selective detection of the products of the atom-ion chemical reactions.

We have subsequently employed the electronic structure data to calculate the rate constants for the elastic scattering as well as radiative charge transfer and radiative

tive association with and without the magnetic field. The relevant temperature scale is set by micromotion in the Paul trap. For $\text{Li}+\text{Yb}^+$, it is less severe than for other species due to the favorable ion to atom mass ratio, limiting the trap temperature to about $10\,\mu\text{K}$ [21–23]. At this temperature, we find clear signatures of Feshbach resonances. This suggests that it should be possible to observe these resonances and use them to control the atom-ion interactions, facilitating sympathetic cooling or molecule formation. This encouraging finding for Yb^+ in Paul trap, immersed in a gas of ultracold Li atoms, is in contrast to many other atom-ion species [61].

Temperatures lower than $10\,\text{mK}$ require sympathetic cooling. Our results suggest a sufficiently large ratio of elastic to inelastic scattering cross sections in the relevant temperature range down to about $10\,\text{nK}$, and thus feasibility of sympathetic cooling. These predictions necessarily come with some uncertainty due to the unknown exact value of the scattering length. A critical assessment of our results reveals that our predictions hold assuming $\pm 5\%$ accuracy of the *ab initio* potentials. We are thus confident to predict the feasibility of the sympathetic cooling of the Yb^+ ion by the Li atoms down to the temperatures of about $10\,\text{nK}$. This implies excellent prospects for building a quantum simulator using Yb^+ ions immersed in a gas of ultracold Li atoms, bringing the quantum simulation of the solid-state physics with AMO experiments a step closer to the reality.

Moreover, since radiative association is found to dominate radiative inelastic processes, $(\text{LiYb})^+$ is also a good candidate for observing ultracold atom-ion chemical reactions. *Controlled* formation of molecular ions becomes possible by applying a laser field, accessing vibrational levels in the ground electronic state as well as electronically excited triplet states. Photoassociation can utilize one-photon transitions to levels with moderate binding energies but the formation of molecular ions in their absolute ground state will require additional Raman transitions.

Our calculated photoassociation spectra are also important for optical trapping since they indicate that photoassociation losses are likely to occur at wavelengths

close to $1064\,\text{nm}$. Since photoassociation lines are typically quite narrow, it should be possible to avoid these losses by proper tuning of the trapping laser. Our calculations indicate in which regions transitions are to be expected but would need to be corroborated by spectroscopy for quantitative predictions.

Molecular ions offer a particularly interesting perspective for the photoassociation and related spectroscopies, in that state-selective detection of a single molecular ion in the trap should be possible. Such a detection scheme can be based on the change of the trapping frequency due to the change of the ion mass when the bond is formed or broken, and state selectivity could be achieved by exploiting the differences in the Stark shifts of different rovibrational levels which modify the trapped-ion spectrum. One could thus envision a series of photoassociation and dissociation experiments, detected by changes in the fluorescence wavelength. Similarly, one can photo-induce, and potentially control, ion-neutral chemical reactions by laser excitation of Li into the 2P state. Due to the favorable shape of the corresponding $^1\Pi$ state, this might provide an alternative and more direct route than photoassociation into the ground electronic state to produce molecular ions in their absolute ground state.

To conclude, $\text{Li}+\text{Yb}^+$ represents an extremely promising example of hybrid atom-ion systems. Good prospects for the sympathetic cooling should allow for its application in quantum simulation in the not too distant future, and several pathways to molecule formation imply interesting avenues for cold controlled chemical reactions.

ACKNOWLEDGMENTS

We would like to thank Tommaso Calarco for bringing our attention to this problem and René Gerritsma for useful discussions. MT and RM thank the Foundation for Polish Science for support within the START and MISTRZ programs, respectively; RM was supported by the Polish Ministry of Science and Education through the project N N204 215539.

-
- [1] D. Leibfried, R. Blatt, C. Monroe, and D. Wineland, *Rev. Mod. Phys.* **75**, 281 (2003).
 - [2] H. Häffner, C. F. Roos, and R. Blatt, *Phys. Rep.* **469**, 155 (2008).
 - [3] R. Blatt and C. F. Roos, *Nat. Phys.* **8**, 277 (2012).
 - [4] C. Zipkes, S. Palzer, C. Sias, and M. Köhl, *Nature* **464**, 388 (2010).
 - [5] C. Zipkes, S. Palzer, L. Ratschbacher, C. Sias, and M. Köhl, *Phys. Rev. Lett.* **105**, 133201 (2010).
 - [6] L. Ratschbacher, C. Zipkes, C. Sias, and M. Köhl, *Nature Phys.* **8**, 649 (2012).
 - [7] L. Ratschbacher, C. Sias, L. Carcagni, J. M. Silver, C. Zipkes, and M. Köhl, *Phys. Rev. Lett.* **110**, 160402 (2013).
 - [8] S. Schmid, A. Härter, and J. H. Denschlag, *Phys. Rev. Lett.* **105**, 133202 (2010).
 - [9] A. T. Grier, M. Cetina, F. Oručević, and V. Vuletić, *Phys. Rev. Lett.* **102**, 223201 (2009).
 - [10] A. Härter, A. Krüchow, A. Brunner, W. Schnitzler, S. Schmid, and J. H. Denschlag, *Phys. Rev. Lett.* **109**, 123201 (2012).
 - [11] K. Ravi, S. Lee, A. Sharma, G. Werth, and S. Rangwala, *Nat. Commun.* **3**, 1126 (2012).
 - [12] F. H. J. Hall, M. Aymar, N. Bouloufa-Maafa, O. Dulieu, and S. Willitsch, *Phys. Rev. Lett.* **107**, 243202 (2011).
 - [13] W. G. Rellergert, S. T. Sullivan, S. Kotochigova, A. Petrov, K. Chen, S. J. Schowalter, and E. R. Hudson, *Phys. Rev. Lett.* **107**, 243201 (2011).

- [14] S. T. Sullivan, W. G. Rellergert, S. Kotochigova, and E. R. Hudson, *Phys. Rev. Lett.* **109**, 223002 (2012).
- [15] R. Gerritsma, A. Negretti, H. Doerk, Z. Idziaszek, T. Calarco, and F. Schmidt-Kaler, *Phys. Rev. Lett.* **109**, 080402 (2012).
- [16] U. Bissbort, D. Cocks, A. Negretti, Z. Idziaszek, T. Calarco, F. Schmidt-Kaler, W. Hofstetter, and R. Gerritsma, *Phys. Rev. Lett.* **111**, 080501 (2013).
- [17] F. H. J. Hall and S. Willitsch, *Phys. Rev. Lett.* **109**, 233202 (2012).
- [18] C. Schneider, M. Enderlein, T. Huber, and T. Schaetz, *Nature Photon.* **4**, 772 (2010).
- [19] C. Cormick, T. Schaetz, and G. Morigi, *New J. Phys.* **13**, 043019 (2011).
- [20] W. Paul, *Rev. Mod. Phys.* **62**, 531 (1990).
- [21] M. Cetina, A. T. Grier, and V. Vuletić, *Phys. Rev. Lett.* **109**, 253201 (2012).
- [22] K. Chen, S. T. Sullivan, and E. R. Hudson, *Phys. Rev. Lett.* **112**, 143009 (2014).
- [23] M. Krych and Z. Idziaszek, arXiv preprint arXiv:1312.0279 (2013).
- [24] R. Gerritsma, private communication.
- [25] M. Tomza, F. Pawłowski, M. Jeziorska, C. P. Koch, and R. Moszynski, *Phys. Chem. Chem. Phys.* **13**, 18893 (2011).
- [26] W. Skomorowski, F. Pawłowski, C. P. Koch, and R. Moszynski, *J. Chem. Phys.* **136**, 194306 (2012).
- [27] M. Krych, W. Skomorowski, F. Pawłowski, R. Moszynski, and Z. Idziaszek, *Phys. Rev. A* **83**, 032723 (2011).
- [28] R. J. Bartlett and M. Musial, *Rev. Mod. Phys.* **79**, 291 (2007).
- [29] P. J. Knowles, C. Hampel, and H.-J. Werner, *J. Chem. Phys.* **99**, 5219 (1993).
- [30] O. Christiansen, H. Koch, and P. Jorgensen, *J. Chem. Phys.* **103**, 7429 (1995).
- [31] H. Koch, O. Christiansen, P. Jorgensen, A. M. S. de Meras, and T. Helgaker, *J. Chem. Phys.* **106**, 1808 (1997).
- [32] S. Boys and F. Bernardi, *Mol. Phys.* **19**, 553 (1970).
- [33] H.-J. Werner, P. J. Knowles, F. R. M. R. Lindh, M. Schütz, P. Celani, T. Korona, G. Rauhut, R. D. Amos, A. Bernhardsson, A. Berning, D. L. Cooper, M. J. O. Deegan, A. J. Dobbyn, E. G. F. Eckert, C. Hampel, G. Hetzer, A. W. Lloyd, S. J. McNicholas, W. Meyer, M. E. Mura, A. Nicklass, P. Palmieri, R. Pitzer, U. Schumann, H. Stoll, A. J. Stone, R. Tarroni, T. Thorsteinsson, M. Wang, and A. Wolf, *MOLPRO, version 2012.1, a package of ab initio programs* (2012), see <http://www.molpro.net>.
- [34] T. Helgaker, H. J. A. Jensen, P. Jorgensen, J. Olsen, K. Ruud, H. Agren, A. A. Auer, K. L. Bak, V. Bakken, O. Christiansen, and et al., “Dalton, an ab initio electronic structure program, release 2.0,” (2005).
- [35] I. S. Lim, H. Stoll, and P. Schwerdtfeger, *J. Chem. Phys.* **124**, 034107 (2006).
- [36] B. Jeziorski and R. Moszynski, *Int. J. Quant. Chem.* **48**, 161 (1993).
- [37] R. Moszynski, P. Zuchowski, and B. Jeziorski, *Collect. Czech. Chem. Commun.* **70**, 1109 (2005).
- [38] T. Korona, M. Przybytek, and B. Jeziorski, *Mol. Phys.* **104**, 2303 (2006).
- [39] A. Derevianko, S. G. Porsev, and J. F. Babb, *At. Data Nucl. Data Tables* **96**, 323 (2010).
- [40] U. I. Safronova and M. S. Safronova, *Phys. Rev. A* **79**, 022512 (2009).
- [41] C. Chen and Z.-W. Wang, *J. Chem. Phys.* **121**, 4171 (2004).
- [42] S. G. Porsev, M. S. Safronova, A. Derevianko, and C. W. Clark, *Phys. Rev. A* **89**, 012711 (2014).
- [43] H. T. C. Stoof, J. M. V. A. Koelman, and B. J. Verhaar, *Phys. Rev. B* **38**, 4688 (1988).
- [44] F. H. Mies, C. J. Williams, P. S. Julienne, and M. Krauss, *J. Res. Natl. Inst. Stand. Technol.* **101**, 521 (1996).
- [45] V. Kokoouline, O. Dulieu, R. Kosloff, and F. Masnou-Seeuws, *J. Chem. Phys.* **110**, 9865 (1999).
- [46] K. Willner, O. Dulieu, and F. Masnou-Seeuws, *J. Chem. Phys.* **120**, 548 (2004).
- [47] S. Kallush and R. Kosloff, *Chem. Phys. Lett.* **433**, 221 (2006).
- [48] B. R. Johnson, *J. Chem. Phys.* **69**, 4678 (1978).
- [49] B. Zygelman and A. Dalgarno, *Phys. Rev. A* **38**, 1877 (1988).
- [50] P. S. Julienne, *J. Chem. Phys.* **68**, 32 (1978).
- [51] J. Tellinghuisen and P. S. Julienne, *J. Chem. Phys.* **81**, 5779 (1984).
- [52] K. Sando and A. Dalgarno, *Mol. Phys.* **20**, 103 (1971).
- [53] R. Napolitano, J. Weiner, C. J. Williams, and P. S. Julienne, *Phys. Rev. Lett.* **73**, 1352 (1994).
- [54] NIST Atomic Spectra Database <http://physics.nist.gov/PhysRefData/ASD>.
- [55] R. W. Molof, H. L. Schwartz, T. M. Miller, and B. Bederson, *Phys. Rev. A* **10**, 1131 (1974).
- [56] W. E. Cooke, T. F. Gallagher, R. M. Hill, and S. A. Edelstein, *Phys. Rev. A* **16**, 1141 (1977).
- [57] V. A. Dzuba and A. Derevianko, *J. Phys. B: At. Mol. Opt. Phys.* **43**, 074011 (2010).
- [58] T. G. A. Heijmen, R. Moszynski, P. E. S. Wormer, and A. van der Avoird, *Mol. Phys.* **89**, 81 (1996).
- [59] P. Pellegrini, M. Gacesa, and R. Côté, *Phys. Rev. Lett.* **101**, 053201 (2008).
- [60] C. Chin, R. Grimm, P. S. Julienne, and E. Tiesinga, *Rev. Mod. Phys.* **82**, 1225 (2010).
- [61] Z. Idziaszek, A. Simoni, T. Calarco, and P. S. Julienne, *New J. Phys.* **13**, 083005 (2011).
- [62] R. Moszynski, B. Jeziorski, A. van der Avoird, and P. E. Wormer, *J. Chem. Phys.* **101**, 2825 (1994).
- [63] P. S. Żuchowski and J. M. Hutson, *Phys. Rev. A* **79**, 062708 (2009).
- [64] W. Skomorowski, M. L. Gonzalez-Martinez, R. Moszynski, and J. M. Hutson, *Phys. Chem. Chem. Phys.* **13**, 19077 (2011).
- [65] T. G. Heijmen, R. Moszynski, P. E. Wormer, A. van der Avoird, A. D. Rudert, J. B. Halpern, J. Martin, W. B. Gao, and H. Zacharias, *J. Chem. Phys.* **111**, 2519 (1999).